RESEARCH ARTICLE

National Science Review
7: 763–774, 2020
doi: 10.1093/nsr/nwz215
Advance access publication 20 December 2019

MATERIALS SCIENCE

$Au_{23}(CR)_{14}$ nanocluster restores fibril Aβ's unfolded state with abolished cytotoxicity and dissolves endogenous Aβ plaques

Wenkang Zhang[1,†], Guanbin Gao[1,†,*], Zhongjie Ma[1], Zhuoying Luo[1], Meng He[2] and Taolei Sun[1,2,*]

ABSTRACT

The misfolding of amyloid-β (Aβ) peptides from the natural unfolded state to β-sheet structure is a critical step, leading to abnormal fibrillation and formation of endogenous Aβ plaques in Alzheimer's disease (AD). Previous studies have reported inhibition of Aβ fibrillation or disassembly of exogenous Aβ fibrils *in vitro*. However, soluble Aβ oligomers have been reported with increased cytotoxicity; this might partly explain why current clinical trials targeting disassembly of Aβ fibrils by anti-Aβ antibodies have failed so far. Here we show that $Au_{23}(CR)_{14}$ (a new Au nanocluster modified by Cys-Arg (CR) dipeptide) is able to completely dissolve exogenous mature Aβ fibrils into monomers and restore the natural unfolded state of Aβ peptides from misfolded β-sheets. Furthermore, the cytotoxicity of $A\beta_{40}$ fibrils when dissolved by $Au_{23}(CR)_{14}$ is fully abolished. More importantly, $Au_{23}(CR)_{14}$ is able to completely dissolve endogenous Aβ plaques in brain slices from transgenic AD model mice. In addition, $Au_{23}(CR)_{14}$ has good biocompatibility and infiltration ability across the blood–brain barrier. Taken together, this work presents a promising therapeutics candidate for AD treatment, and manifests the potential of nanotechnological approaches in the development of nanomedicines.

Keywords: gold nanoclusters, Alzheimer's disease, restores fibril Aβ's unfolded state, abolished cytotoxicity, dissolves endogenous Aβ plaques

[1]State Key Laboratory of Advanced Technology for Materials Synthesis and Processing, Wuhan University of Technology, Wuhan 430070, China and [2]School of Chemistry, Chemical Engineering and Life Science, Wuhan University of Technology, Wuhan 430070, China

***Corresponding authors**. E-mails: gbgao@whut.edu.cn; suntl@whut.edu.cn
†Equally contributed to this work.

Received 16 October 2019; **Revised** 4 December 2019; **Accepted** 6 December 2019

INTRODUCTION

A hallmark sequence of events in Alzheimer's disease (AD) is the misfolding, fibrillation and accumulation of amyloid-β (Aβ) peptides, resulting in cellular dysfunction, loss of synaptic connections and brain damage [1–4]. Over the past three decades, the inhibition of Aβ fibrillation and the disassembly of deposited Aβ fibrils have been the magnets for searching promising therapeutics for AD treatment [5–9]. A number of inhibitors (including β- and γ-secretase inhibitors) for inhibiting Aβ production were discontinued in phase ii or iii clinical trials due to their low efficacy and serious side effects [10]. Anti-Aβ antibody-based immunotherapy for disassembling the mature Aβ fibrils was once expected to be the first radical treatment of AD [11]. However, prior studies have indicated that the soluble Aβ oligomers, as the most toxic species, might reappear during the disassembly process to induce more neurotoxicity (i.e. the 'dust-raising' effect) [12–16]. One approach to ameliorate the toxicity of soluble Aβ oligomers is to promote their aggregation by, for example, chiral silica nanoribbons and star-shaped poly(2-hydroxyethyl acrylate) nanostructures [17,18]. Also, graphene quantum dots are reported to drive the peptide fibrillization off-pathway to eliminate the toxic intermediates, which points to the potential of using zero-dimensional nanomaterials for *in vivo* mitigation of a range of amyloidosis types [19]. Recently, polymer-peptide conjugates and curcumin–gold nanoparticles (AuNPs) with hydrodynamic diameters of 10–25 nm have been shown to disassemble exogenous Aβ fibrils *in vitro*, but they failed to restore the natural unfolded state of Aβ from the misfolded β-sheets [20–22]. However, the β-lactoglobulin 'coronae' of the

AuNPs are reported to enable X-ray destruction of islet amyloid polypeptide (IAPP) amyloids, providing a viable new nanotechnology against amyloidogenesis [23]. The small molecule epigallocatechin gallate (EGCG) presents the capability to prevent aggregation and remodel amyloid fibrils, which could also convert mature amyloid fibrils to amorphous protein aggregates that are less toxic to cells, implying the possibility of reducing the toxicity of amyloid fibrils by remodeling their molecular structures [24–26]. Therefore, the treatment of AD needs to explore new materials that are able to dissolve endogenous Aβ plaques and abolish the proteotoxicity of Aβ fibrils by restoring their natural unfolded state from the misfolded β-sheets.

To date, nanomaterials and multifunctional nanocomposites possessing certain structural and physicochemical traits are promising candidates for mitigating amyloidosis *in vitro* and *in vivo*, indicating the use of nanoparticles as an emerging field against amyloid diseases [16,27]. Gold nanoclusters (AuNCs) ($d < 3$ nm) have been widely studied in biomedical fields due to their small-size effect and good biocompatibility [28–30]. Our previous study has shown that glutathione-modified AuNCs (GSH-AuNCs) can completely inhibit the fibrillation of Aβ peptides [31,32]. This study was expanded to explore whether any AuNCs including GSH-AuNCs could dissolve mature exogenous Aβ fibrils and endogenous Aβ senile plaques, and, more importantly, restore the natural unfolded state of Aβ from the misfolded β-sheets. To this end, seven kinds of AuNCs (i.e. Cys-AuNCs, CSH-AuNCs, *p*-MBA-AuNCs, MPA-AuNCs, GSH-AuNCs, NIBC-AuNCs and CR-AuNCs) modified by cysteine, cysteamine, 4-mercaptobenzoic acid, mercaptopropionic acid, glutathione, *N*-isobutyryl-*L*-cysteine or Cys-Arg, respectively, have been synthesized.

RESULTS AND DISCUSSION

Seven kinds of AuNCs on inhibiting Aβ fibrillation

First, the effects of these seven kinds of AuNCs on inhibiting Aβ fibrillation were investigated by co-incubating 20 μmol·L^{-1} Aβ_{40} with each kind of AuNCs at the same concentration (25 mg·L^{-1}). The concentrations were selected based on their solubility and biological relevance from our preliminary experiments. The standard thioflavine-T (ThT) binding fluorescence assay was employed to record the fibrillation kinetics. As shown in Fig. 1A, the fibrillation kinetics of 20 μmol·L^{-1} Aβ_{40} without AuNCs showed a standard S-curve (black curve); the formation of preformed/mature Aβ_{40} fibrils was confirmed by atomic force microscopy (AFM) images (Fig. 1B; Fig. S1 in the online supplementary material). Cys-AuNCs had no inhibitory effect (red curve); CSH-AuNCs (orange curve), *p*-MBA-AuNCs (yellow curve) and MPA-AuNCs (green curve) showed partial inhibition. Consistent with our previous studies, GSH-AuNCs showed complete inhibition of Aβ_{40} fibrillation (blue curve). Encouragingly, NIBC-AuNCs (cyan curve) and CR-AuNCs (purple curve) were also able to completely inhibit Aβ_{40} fibrillation, which was further verified by AFM images (no fibrils could be found in Fig. 1C–E). Moreover, *in situ* real-time circular dichroism (CD) spectra were used to record the conformational transition of Aβ_{40} in the fibrillation process. As shown in Fig. 1F, in the absence of AuNCs, Aβ_{40} had undergone a misfolding process from an unfolded state (negative peak at 198 nm) into a β-sheet structure (negative peak at 220 nm). Interestingly, GSH-AuNCs (Fig. 1G), NIBC-AuNCs (Fig. 1H) and CR-AuNCs (Fig. 1I) could maintain the unfolded state of Aβ_{40} peptides throughout the incubation. It should be noted that the seven AuNCs used have similar particle sizes (1.6 ± 0.5 nm), and their transmission electron microscope (TEM) images and the UV-visible absorption spectra are shown in Fig. S2.

Seven kinds of AuNCs on the dissolving of mature Aβ fibrils

Since inhibition of fibrillation and dissolution of fibrils should be considered as two discrete events, then whether these AuNCs could dissolve preformed/mature Aβ_{40} fibrils was investigated by using CD and AFM. Freshly prepared Aβ_{40} (20 μmol·L^{-1}) were pre-incubated at 37°C for 72 h. The preformed Aβ_{40} fibrils were then co-incubated with 50 mg·L^{-1} individual AuNCs for 48 h. The formation and dissolution of Aβ_{40} fibrils were recorded by CD. The data showed that the peak at 220 nm did not change between 72 h and 120 h when treated with Cys-AuNCs (Fig. 2B$_1$), CSH-AuNCs (Fig. 2C$_1$), *p*-MBA-AuNCs (Fig. 2D$_1$), MPA-AuNCs (Fig. 2E$_1$), GSH-AuNCs (Fig. 2F$_1$) and NIBC-AuNCs (Fig. 2G$_1$), and that the fibrils were intact (Fig. 2B$_2$–G$_2$), indicating no dissolution of the mature Aβ_{40} fibrils. The failure of GSH-AuNCs to dissolve Aβ_{40} fibrils confirmed that inhibition of fibrillation and dissolution of fibrils are two discrete events. Most excitingly, when treated by CR-AuNCs, the peak at 220 nm (i.e. β-sheet) disappeared and the peak at 198 nm (i.e. unfolded state) resurfaced (Fig. 2H$_1$). The dissolution of

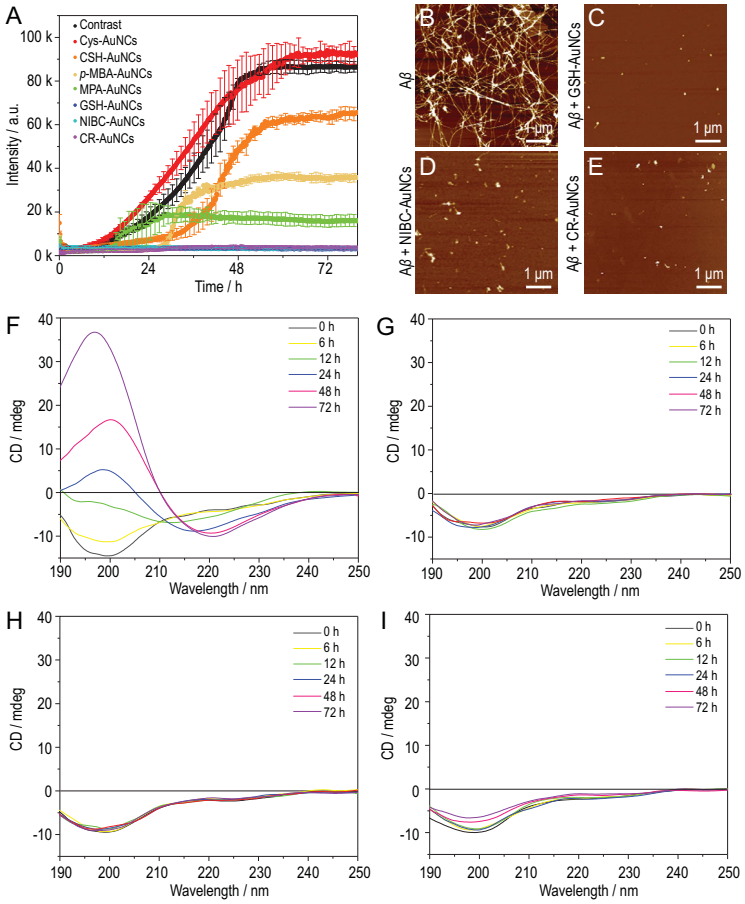

Figure 1. (A) Fibrillation kinetics for 20 μmol·L^{-1} Aβ_{40} in the absence (black) or presence of 25 mg·L^{-1} Cys-AuNCs, CSH-AuNCs, *p*-MBA-AuNCs, MPA-AuNCs, GSH-AuNCs, NIBC-AuNCs or CR-AuNCs. (B–E) AFM images of Aβ_{40} after 72 h co-incubation in the absence (B) or presence of 25 mg·L^{-1} GSH-AuNCs (C), NIBC-AuNCs (D) and CR-AuNCs (E). (F–I) *In situ* real-time CD spectra monitoring of 20 μmol·L^{-1} Aβ_{40} peptides co-incubated without (F) or with 25 mg·L^{-1} GSH-AuNCs (G), NIBC-AuNCs (H) and CR-AuNCs (I) for 72 h.

the mature Aβ_{40} fibrils by CR-AuNCs was further confirmed by AFM observation (Fig. 2H$_2$). The perfect overlay of CD curves of 0 h and 120 h demonstrated that CR-AuNCs could completely dissolve the mature Aβ_{40} fibrils, and fully restore the unfolded state of Aβ_{40} peptides from β-sheet structure.

Molecular composition and structure of CR-AuNCs

To ascertain their molecular composition and structure, CR-AuNCs were characterized using various technical platforms (Fig. 3 and Fig. S3). The electrospray ionization mass spectrometry (ESI-MS) analysis showed a single distinct peak at 8397.9925, indicating that CR-AuNCs had a formula of $Au_{23}(CR)_{14}$ (Fig. 3A). The formula was further confirmed by thermogravimetric analysis (Fig. 3B). The weight loss of 46.0% meant that the CR weight ratio agrees well with the formula of $Au_{23}(CR)_{14}$ (calculated loss: 46.0%). In addition, the high resolution TEM analysis showed that the $Au_{23}(CR)_{14}$ had a spherical morphology (Fig. 3C), where the shape was regular with a clear lattice fringe (inset of Fig. 3C).

The process detail and possible mechanisms of $Au_{23}(CR)_{14}$ dissolving the preformed Aβ_{40} fibrils

To gain more insights into the dissolution process, preformed Aβ_{40} fibrils were co-incubated with 50 mg·L^{-1} $Au_{23}(CR)_{14}$ for 48 h. The dissolution dynamics were monitored by ThT assay. The fluorescence intensity declined continuously during 48 h incubation (Fig. 4A), indicating a gradual process of dissolution. The gradual dissolution of Aβ_{40} fibrils had also been evidenced by AFM studies (Fig. 4B$_1$–B$_6$). The apparent sizes of the samples were assayed by dynamic light scattering (DLS). The DLS results showed that the apparent sizes of the samples decreased from over 1000 nm to less than 10 nm (Fig. 4C$_1$–C$_6$). The *in situ* real-time CD spectra revealed that the peak at 220 nm was continuously shifted to 198 nm (Fig. 4D), indicating that the dissolution of Aβ_{40} fibrils by $Au_{23}(CR)_{14}$ is a dynamic process accompanied by a conformational transition from a β-sheet structure to an unfolded state. The native PAGE results showed one band with a molecular weight less than 6.5 kDa (Fig. 4E, 48 h), directly demonstrating that $Au_{23}(CR)_{14}$ completely dissolves Aβ_{40} fibrils into monomers (~4.2 kDa).

To explore possible mechanisms of how $Au_{23}(CR)_{14}$, but not the other six kinds of AuNCs, could dissolve Aβ_{40} fibrils, the zeta potentials of Aβ_{40} fibrils, individual AuNCs and Aβ_{40} fibrils, together with individual AuNCs, were measured. The median of the zeta potential of mature Aβ_{40} fibrils was -41 ± 2 mV (black curves in Fig. 4F and Fig. S4). Cys-AuNCs, CSH-AuNCs, *p*-MBA-AuNCs, MPA-AuNCs, GSH-AuNCs, NIBC-AuNCs and $Au_{23}(CR)_{14}$ have a zeta potential of -32, $+36$, -49, -57, $+2$, -34 and $+68$ mV, respectively (blue curves in Fig. 4F and Fig. S4). After addition of AuNCs, while the mixtures with the other six kinds of AuNCs showed a negative zeta potential with a median value from -44 to -18 mV, the mixture with $Au_{23}(CR)_{14}$ showed a positive zeta potential with a median value of $+34$ mV (red curves in Fig. 4F and Fig. S4). These data suggest that $Au_{23}(CR)_{14}$ adsorb onto

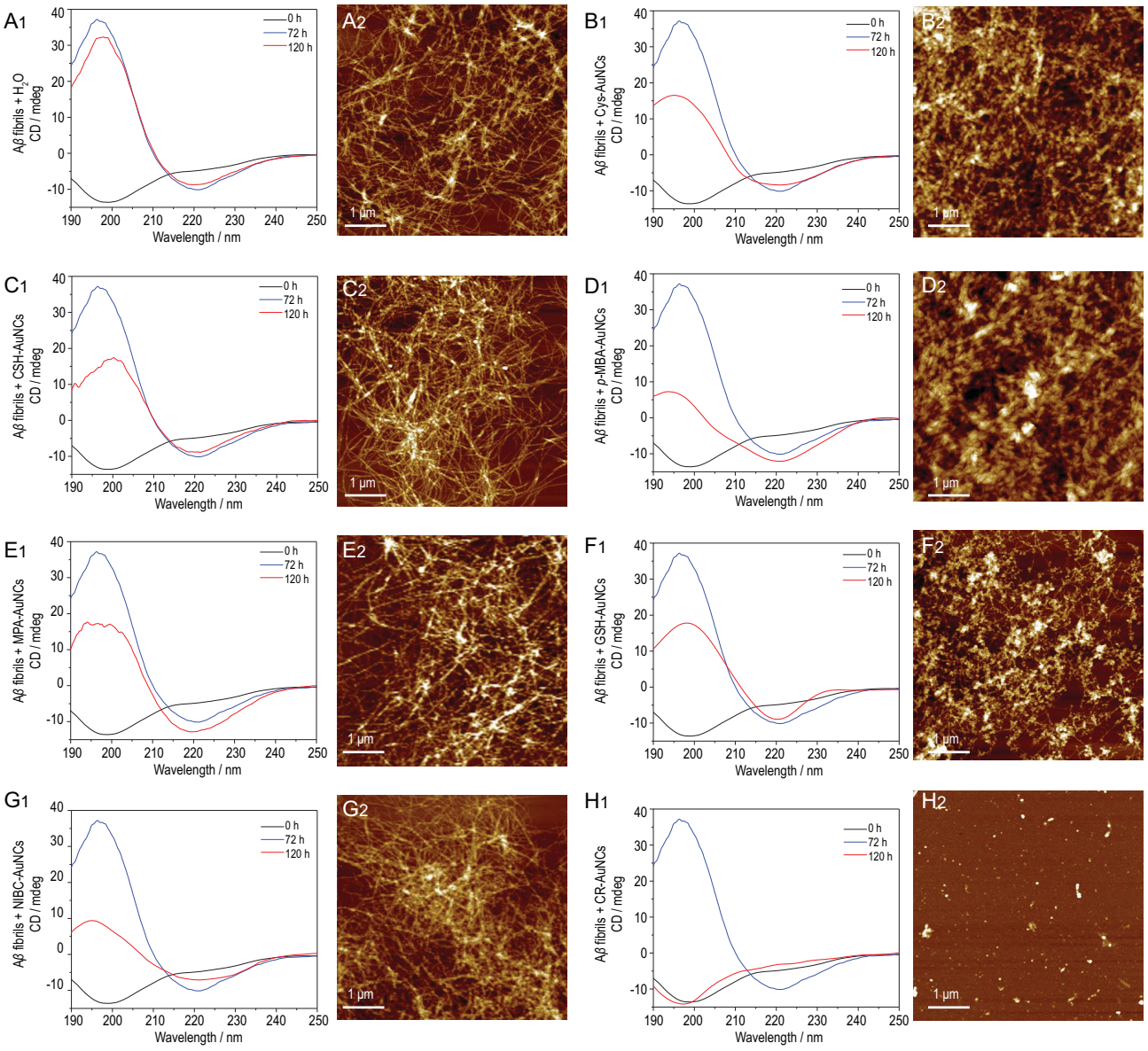

Figure 2. (A_1–H_1) CD spectra of 20 μmol·L^{-1} Aβ_{40}: black curves (0 h) denoting 0 h prior to incubation; blue curves (72 h) denoting pre-incubation for 72 h; red curves (120 h) denoting the co-incubation for 48 h of preformed Aβ_{40} fibrils in the (A_1) absence or presence of 50 mg·L^{-1} (B_1) Cys-AuNCs, (C_1) CSH-AuNCs, (D_1) *p*-MBA-AuNCs, (E_1) MPA-AuNCs, (F_1) GSH-AuNCs, (G_1) NIBC-AuNCs and (H_1) CR-AuNCs. (A_2–H_2) AFM images of the samples at the end of CD experiments (120 h): (A_2) blank control, (B_2) Cys-AuNCs, (C_2) CSH-AuNCs, (D_2) *p*-MBA-AuNCs, (E_2) MPA-AuNCs, (F_2) GSH-AuNCs, (G_2) NIBC-AuNCs and (H_2) CR-AuNCs.

Aβ_{40} fibrils more strongly than other AuNCs. In consideration of Aβ_{40} monomers with a net charge of negative 2.7 at physiological pH (7.4) [33], and the existence of a guanidine group in the residue of CR that could be protonated in a wide range of pH [34], the strong electrostatic interaction between Aβ_{40} and $Au_{23}(CR)_{14}$ might drive the gradual dissolution of mature Aβ_{40} fibrils. The above results strongly suggest that $Au_{23}(CR)_{14}$ dissolve the preformed/mature Aβ_{40} fibrils from misfolded β-sheets into the unfolded monomer state through strong electrostatic interactions.

$Au_{23}(CR)_{14}$-mediated Aβ_{40} fibril dissolution on cell viabilities

To investigate the effect of $Au_{23}(CR)_{14}$-mediated dissolution of Aβ_{40} fibrils on cell viabilities, an AD cell model based on Aβ_{40} fibril-induced cell deaths of PC-12 cells was adopted [35]. First, PC-12 cells were co-incubated with freshly preformed Aβ_{40} fibrils without (Fig. 5A) or with (Fig. 5B) $Au_{23}(CR)_{14}$, and *in situ* real-time morphological changes were recorded by a Cytation 5 Cell Imaging Multi-Mode Reader. Aβ_{40} fibrils formed from

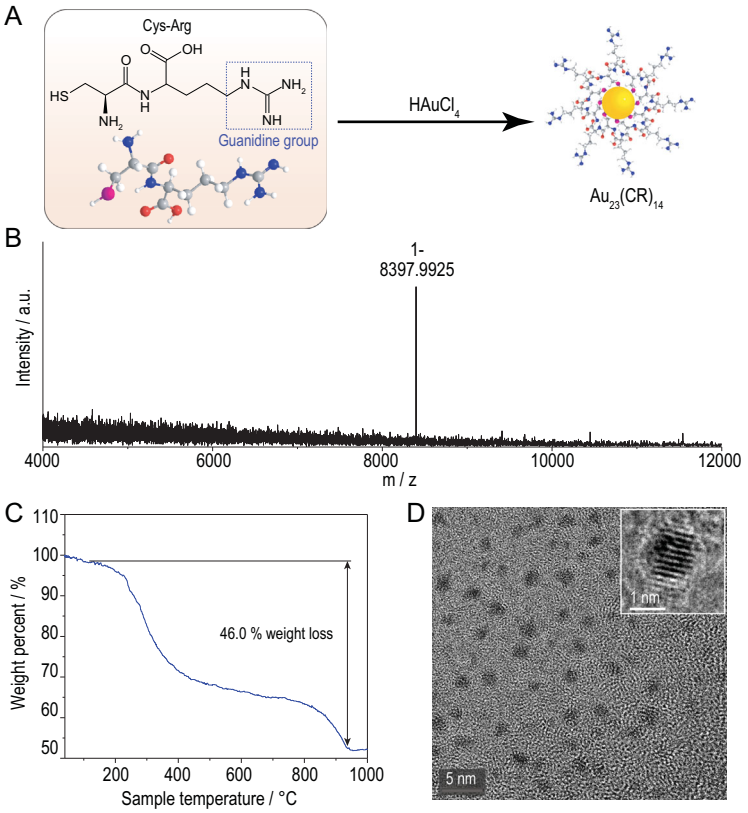

Figure 3. (A) Scheme of synthesis of CR-AuNCs and characterization of CR-AuNCs by (B) ESI-MS analysis, (C) thermogravimetric analysis and (D) TEM image.

20 μmol·L^{-1} monomers were used to cause a 50% decrease of cell viability based on our preliminary titration experiments. As shown in Fig. 5A, when treated with Aβ_{40} fibrils alone, cell shrinkage started to appear in the 3rd hour, and then cells with reduced sizes and round shapes apparently increased from the 12th to the 48th hour. In contrast, when PC-12 cells were treated with Aβ_{40} fibrils and 50 mg·L^{-1} $Au_{23}(CR)_{14}$, no obvious morphological changes were observed (Fig. 5B). The corresponding videos are shown in the online supplementary material. Second, a CCK-8 assay was used for quantifying cell viabilities. Freshly preformed Aβ_{40} fibrils from 20 μmol·L^{-1} monomers were added into PC-12 cells with or without $Au_{23}(CR)_{14}$; the cells were cultured and sampled at the 3rd, 6th, 12th, 24th and 48th hour for assaying their viabilities. No treatment was included as the blank control. As shown in Fig. 5C, the cell viability was not affected in the blank control group (gray bars), and the addition of preformed Aβ_{40} fibrils alone caused a gradual decrease of cell viability to 50% (red bars). In contrast, when cells were cultured with 50 mg·L^{-1} $Au_{23}(CR)_{14}$ together with preformed Aβ_{40} fibrils, the cell viability decreased initially to 70% at the 12th hour and then started to increase, reaching almost 100% (same as the blank control) at the 48th hour (blue bars). These data collectively demonstrated that $Au_{23}(CR)_{14}$ could fully abolish the cytotoxicity of Aβ_{40} fibrils. As for the two phasic characteristics of cell viabilities in the $Au_{23}(CR)_{14}$ treatment, we speculate that the toxic oligomers [36,37] were produced during the dissolution process and the cytotoxicity was fully abolished when the oligomers were completely dissolved into non-toxic monomers.

The capacity of $Au_{23}(CR)_{14}$ for dissolving exogenous Aβ fibrils

The ultimate test is whether the capacity of $Au_{23}(CR)_{14}$ for dissolving exogenous Aβ fibrils can be translated into dissolving the endogenous Aβ plaques. We obtained brain slices derived from the resected brain tissue of an adult transgenic mouse model of AD, where the brain slices contained endogenous Aβ plaques. The brain slices were co-incubated without (Fig. 6A_1–A_3) or with (Fig. 6B_1–B_3) $Au_{23}(CR)_{14}$ for 24 h, and then the slices were stained with anti-Aβ antibodies for immunohistochemical analyses. Figure 6A_1–A_3 shows that the hippocampus and the neocortex were present with a large amount of endogenous Aβ plaques (yellow-brown patches indicated by the arrows). Excitingly, the treatment with 50 mg·L^{-1} $Au_{23}(CR)_{14}$ eliminated all yellow-brown patches (Fig. 6B_1–B_3), demonstrating that $Au_{23}(CR)_{14}$ could completely dissolve the endogenous Aβ plaques in the hippocampus and the neocortex. Furthermore, our data showed that $Au_{23}(CR)_{14}$ did not affect cell viability at a concentration of as high as 100 mg·L^{-1} (Fig. S5), indicating good biocompatibility. In addition, the overcoming of the blood–brain barrier is one precondition of nanomaterials in treating neurological diseases [6]. Our data showed that $Au_{23}(CR)_{14}$ particles were readily detected in the brain tissues when intraperitoneally injected into normal mice, demonstrating that $Au_{23}(CR)_{14}$ is capable of overcoming the blood–brain barrier (Fig. 6D).

CONCLUSION

In conclusion, seven kinds of AuNCs (i.e. Cys-AuNCs, CSH-AuNCs, *p*-MBA-AuNCs, MPA-AuNCs, GSH-AuNCs, NIBC-AuNCs and $Au_{23}(CR)_{14}$) were synthesized and adopted to investigate their effects on the dissolution of mature Aβ fibrils and the restoration of the unfolded state of Aβ peptides. Among the seven kinds of AuNCs tested, only $Au_{23}(CR)_{14}$ are able to completely dissolve exogenous mature Aβ fibrils

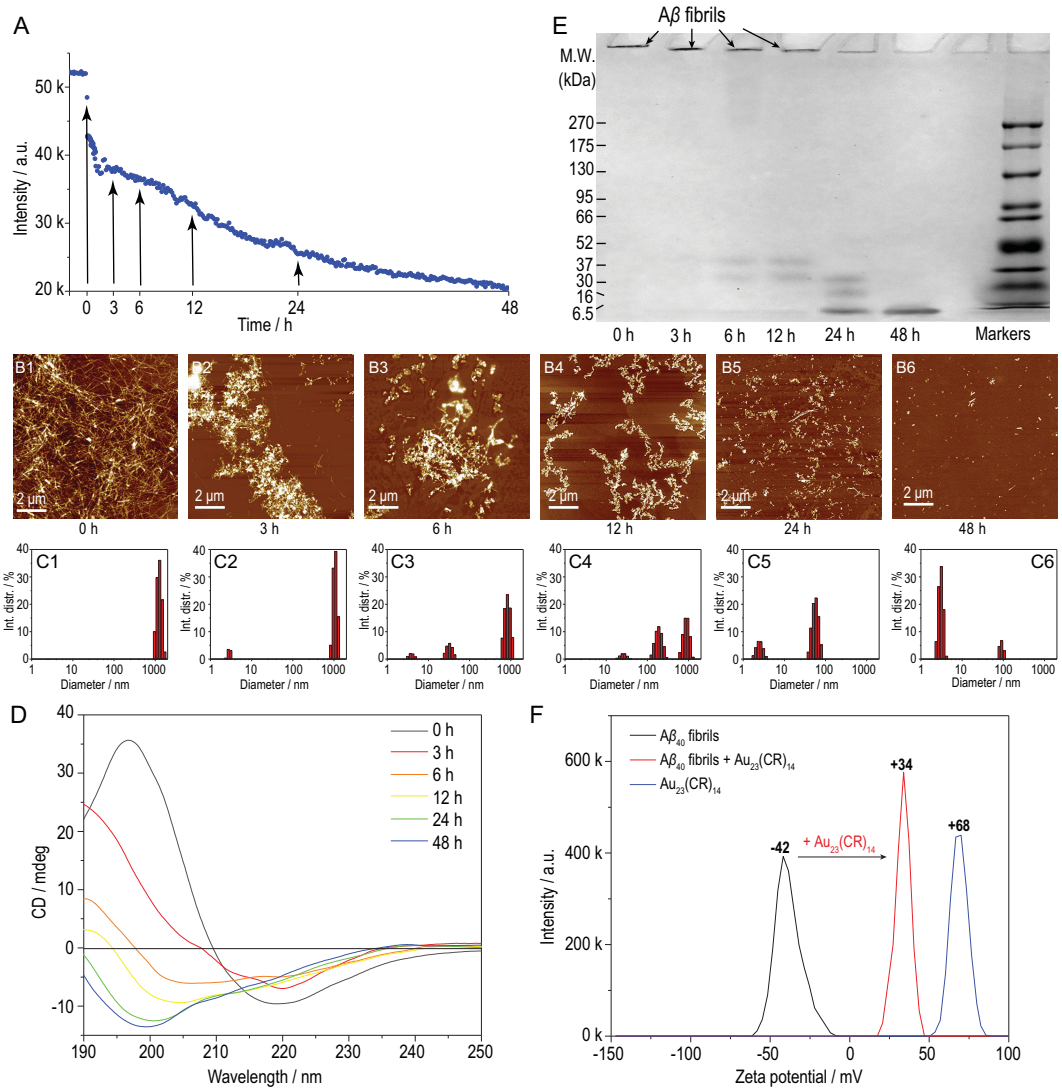

Figure 4. (A) The kinetics of Aβ_{40} fibrils co-incubated with 50 mg·L^{-1} $Au_{23}(CR)_{14}$ for 48 h. (B) AFM images of Aβ_{40} fibrils co-incubated with 50 mg·L^{-1} $Au_{23}(CR)_{14}$ for (B_1) 0 h, (B_2) 3 h, (B_3) 6 h, (B_4) 12 h, (B_5) 24 h and (B_6) 48 h. (C) DLS results of Aβ_{40} fibrils co-incubated with 50 mg·L^{-1} $Au_{23}(CR)_{14}$ for (C_1) 0 h, (C_2) 3 h, (C_3) 6 h, (C_4) 12 h, (C_5) 24 h and (C_6) 48 h. (D) *In situ* real-time CD spectra of 20 μmol·L^{-1} Aβ_{40} fibrils co-incubated with 50 mg·L^{-1} $Au_{23}(CR)_{14}$. (E) Native PAGE gel electrophoresis analysis of $Au_{23}(CR)_{14}$-treated preformed Aβ_{40} fibrils for designated times. (F) Zeta potential of preformed Aβ_{40} fibrils immediately after the injection of $Au_{23}(CR)_{14}$.

into monomers, and fully abolish cytotoxicity by restoring the natural unfolded state of Aβ peptides from misfolded β-sheets. Furthermore, $Au_{23}(CR)_{14}$ are able to completely dissolve endogenous Aβ plaques in the brain slices from transgenic AD model mice. In addition, $Au_{23}(CR)_{14}$ have good biocompatibility and infiltration ability across the blood–brain barrier. The biodistribution of AuNCs *in vivo* has been reported in our recent paper published in *Nanomedicine* [38]. Compared with the chaperone-gold nanoparticle *in vivo* test on zebrafish, similar efficacies to dissolve Aβ plaques and cross the blood–brain barrier are achieved by $Au_{23}(CR)_{14}$ based on a rodent model, further indicating the clinical potential of nanoparticles or nanoclusters against Alzheimer's symptoms [39]. The relevant behavioral pathology and neurodegeneration would be offered in subsequent research. This study provides a compelling nanotherapeutic candidate for AD treatment.

METHODS

Materials, cells and mice

Amyloid β Protein Fragment 1–40 (Aβ_{40}) peptides powder (≥90%), chloroauric acid ($HAuCl_4 \cdot 3H_2O$, 99.999%), *L*-cysteine (≥97%), cysteamine

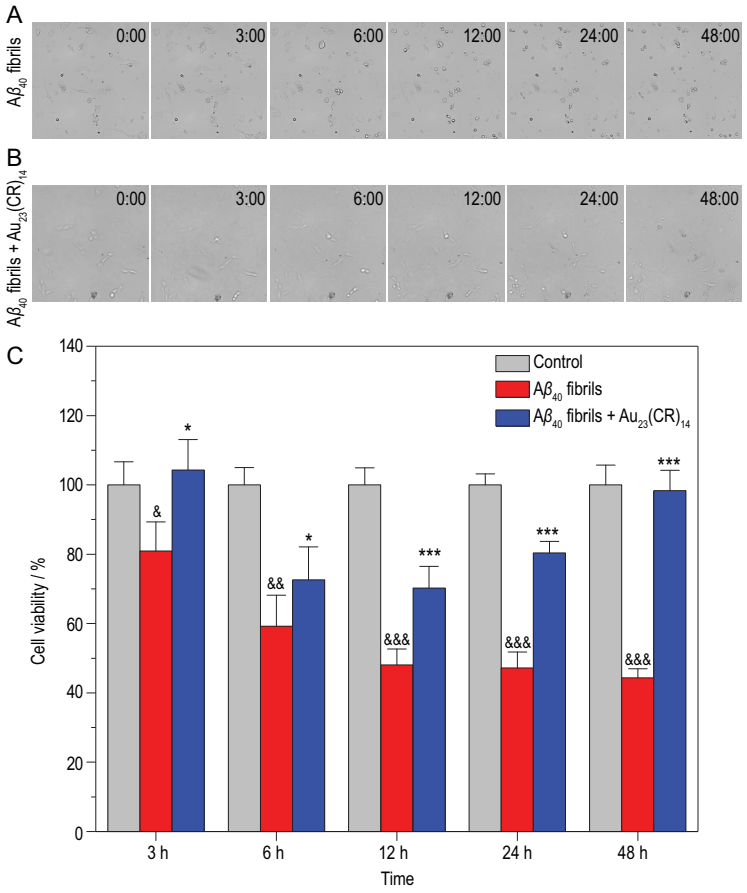

Figure 5. (A, B) *In situ* real-time morphological changes of PC-12 cells co-incubated with freshly preformed Aβ_{40} fibrils without (A) or with 50 mg·L^{-1} $Au_{23}(CR)_{14}$ (B). (C) Viabilities of PC-12 cells after Aβ_{40} fibril treatment in the absence (red) and presence (blue) of 50 mg·L^{-1} $Au_{23}(CR)_{14}$ for 3, 6, 12, 24 and 48 h. No treatment was included as the blank control (gray). Student's *t*-test: $n = 5$, $^{*}P < 0.05$, $^{***}P < 0.001$ vs. Aβ_{40} fibrils-induced group; $^{\&}P < 0.05$, $^{\&\&}P < 0.01$, $^{\&\&\&}P < 0.001$ vs. control.

(≥98%), 4-mercaptobenzoic acid (≥99%), mercaptopropionic acid (≥99%), glutathione (≥98%), *N*-isobutyryl-*L*-cysteine (≥97%) and 2-(2-methoxy-4-nitrophenyl)-3-(4-nitrophenyl)-5-(2,4-disulfophenyl)-2*H*-tetrazolium sodium salt (CCK-8) were purchased from Sigma-Aldrich Co. Ltd. (NJ, USA). Sodium borohydride ($NaBH_4$, ≥96.0%), DMEM, hydrochloric acid, anhydrous ethanol, anhydrous methanol, sodium hydroxide, glacial acetic acid and sulfuric acid were analytical grade and all from Innochem (China). Cys-Arg (97%) was purchased from ChinaPeptides (Shanghai, China). The ultrapure water used was from the Millipore Milli-Q ultrapure water system. All the reaction vessels were soaked in aqua regia (volume ratio = 3:1, HCl/HNO_3) for 24 h, washed thoroughly with ultrapure water several times and dried in an oven before use. The PC-12 cell line was purchased from the Cell Bank of Chinese Academy of Sciences (Beijing). APPswe/PSdE9 double transgenic mice (APP/PS1 Tg mice, 35 weeks of age) and C57BL/6 wild-type mice (9 weeks of age) were obtained from the Model Animal Research Center of Nanjing University (China). All animal experiments were approved by the Animal Ethics Committee, Wuhan University of Technology.

Synthesis and characterizations of Cys-Arg dipeptide

Cys-Arg dipeptides were synthesized by peptide synthesizer (LibertyBlue) [40]. Purity analysis was performed on high performance liquid chromatography (HPLC, Waters 2695). The stationary phase was a 4.6 × 250 mm chromatographic column (Kromasil, C18-5). The flow rate was adjusted to 1.0 mL·min^{-1}; 5 μL of sample was injected at room temperature. Gradient elution was performed using 0.1% trifluoroacetic acid in 100% acetonitrile (Solvent A) and 0.1% trifluoroacetic acid in 100% water (Solvent B) with the following gradient combination: 0.01 min, 1A/99B; 25 min, 26A/74B; 25.1 min, 100A/0B; and 30 min, stop. Detection was performed at 220 nm. Then, the purified products (CR ligand) were characterized by ^{1}H NMR in DMSO-d_6 (Bruker BioSpin GmbH 500 MHz). Next, characterized by mass spectrometry (MS), the purified CR ligands were dissolved in a 50:50 (%) (v/v) acetonitrile/water mixture. The flow rate of electrospray for the dissolved sample was 0.2 mL·min^{-1}, using nebulizer gas (nitrogen) with a flow rate of 1.5·L min^{-1} and block temperature of 200°C. Positive-mode ESI-MS were used for analysis with −4.5 kV probe bias.

Synthesis of AuNCs with different ligands

All AuNCs used in this work were synthesized on the basis of a method reported in our previous study with only a few minor changes in experimental parameters [19,30]. Take $Au_{23}(CR)_{14}$ for example, 0.675 mmol (187 mg) of CR was dissolved in a 100 mL mixture of ultrapure water and ethyl alcohol (v/v = 1/2). Then a freshly prepared aqueous solution (6 mL) of $HAuCl_4$ (2.5 mmol·L^{-1}) was slowly added into the pre-prepared mixture. The mixed solution was cooled to ~0°C in a cool bath for 18 h under a proper stirring frequency (340 rpm by mechanical agitation). Then, a fresh aqueous solution of NaOH (0.1 mol·L^{-1}, 18 mL) was added to the mixed solution. The reaction was maintained for 10 min and stirred vigorously (400 rpm). A freshly prepared aqueous solution of $NaBH_4$ (0.11 mol·L^{-1}, 200 μL) was cooled to 4°C and added rapidly to the mixed solution. Another 1 h was needed for the mixed

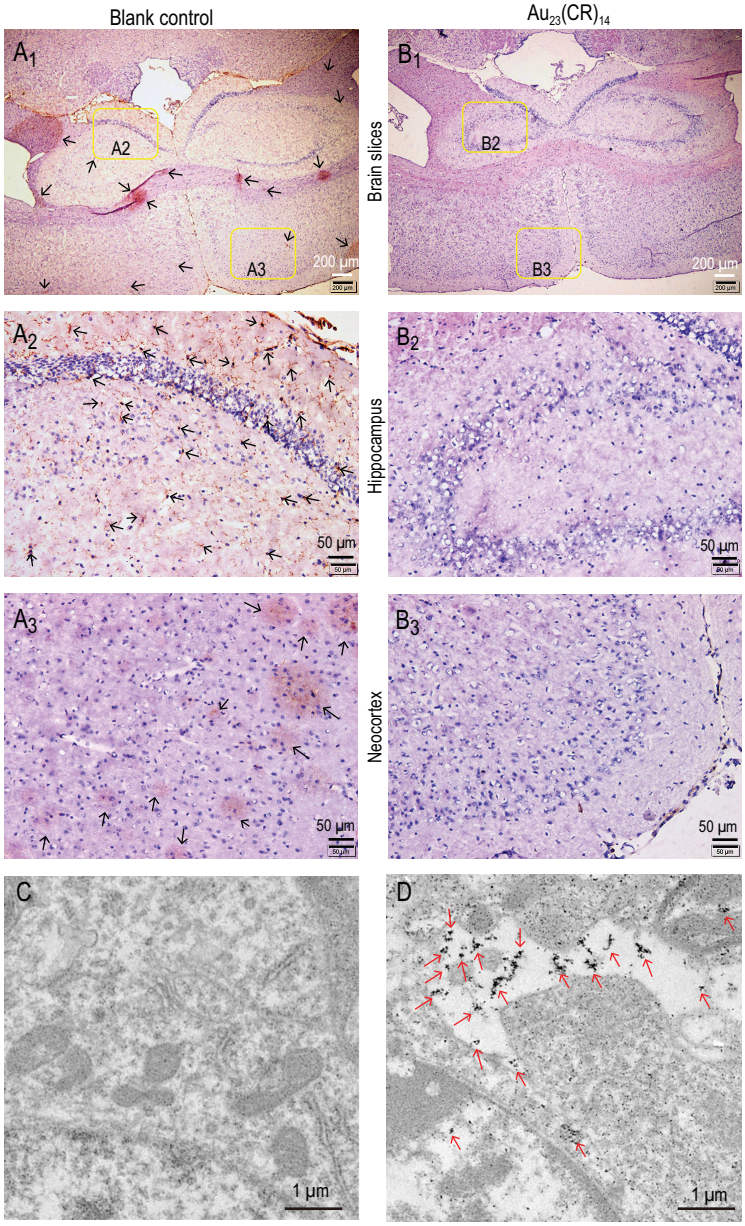

Figure 6. Immunohistochemical analyses of the hippocampus and the neocortex in the brain slices of AD model mice. The brain slices were co-incubated without (A) or with (B) 50 mg·L^{-1} $Au_{23}(CR)_{14}$ for 24 h after fixing on the glass slides. (A2) and (B2) are the partial enlargement of hippocampus. (A3) and (B3) are the partial enlargement of neocortex. (C, D) TEM images of the mouse slices at 6 h after intraperitoneal injection of $Au_{23}(CR)_{14}$ with a dose of 20 mg·kg^{-1} (D) or same volume of normal saline (C) in the normal mice. The presence of $Au_{23}(CR)_{14}$ is marked by red arrows.

solution to react completely. The resulting mixed solution was collected and moved into an Amicon® Ultra-4 3K (MWCO: 3000) Centrifugal Filter device for centrifugal separation (RCF: 5000 × g, 30 min). Then the solution in the centrifuge tube was removed, and the solution in the filter device was washed by ultrapure water several times. Finally, the $Au_{23}(CR)_{14}$ solution in the filter device was collected and lyophilized for further characterizations and experiments. The other six kinds of AuNCs were synthesized following similar conditions and operations.

Characterization

Nuclear magnetic resonance spectroscopy measurements

Hydrogen (^{1}H) nuclear magnetic resonance (H-NMR) spectra of CR dipeptide were recorded on a Bruker AVANCE III 500 MHz spectrometer. A 100 mg·L^{-1} sample solution was added to the NMR tube, and the data were analysed by MestReNova.

Infrared spectroscopy measurements

Infrared (IR) spectra of AuNCs and the corresponding ligands were recorded on a Bruker Vertex 80v Fourier transform infrared (FT-IR) spectrometer. Lyophilized AuNCs and the corresponding ligands were directly used for IR measurement with ATR mode in a vacuum atmosphere at room temperature. Scanning range: 4000–400 cm^{-1}; scan times: 64; vacuum degree: <5 hPa.

UV–visible spectroscopy measurements

UV–visible spectra of AuNCs were recorded on a Shimadzu UV-1800 UV-Vis spectrophotometer with a range of 300–1000 nm at a scan rate of 0.5 nm·s^{-1}. Lyophilized AuNCs were dissolved in water and then diluted to 200 μL with a concentration of 200 mg·L^{-1}. Then the sample was transferred into a high-quality quartz glass cuvette with a black wall for spectrophotometry (volume: 600 μL).

Mass spectrometry measurements

ESI-MS of CR-AuNCs was performed on a Nano electrospray ionization-quadrupole time-of-flight mass spectrometer (ESI-Q-TOF MS, Bruker) operating in the negative ion mode. The sample injection rate was 8 μL·min^{-1}. A capillary voltage of 4 kV was used for the ESI-MS (nebulizer: 1.5 bar, dry gas: 4 L·min^{-1}, 120°C, m/z = 800–12 000). The ESI-MS spectra were obtained by accumulating for 5 min.

Thermal gravimetric analysis measurements

Thermal gravimetric analysis (TGA) was performed on a SETARAM TG-DSC 111 instrument. The sample was dried before TG measurement. The test was performed in flowing air with a temperature increasing rate of 1°C·min^{-1}.

X-ray photoelectron spectroscopy analysis

X-ray photoelectron spectroscopy (XPS) measurements were performed by an ESCALAB 250Xi with a focused monochromatic Al Kα X-ray (1350 eV) source for excitation. The binding energy (BE) scale is calibrated by using the O 1s peak at 530.14 $\pm$ 0.05 eV, the N 1s peak at 400.06 $\pm$ 0.05 eV, the C 1s peak at 283.42 $\pm$ 0.05 eV, the S 2p peak at 161.47 $\pm$ 0.05 eV and the Au 4f peak at 83 $\pm$ 0.05 eV for known reference foils.

TEM measurements

The TEM measurements of AuNCs were performed by using a Talos F200S TEM (Thermo Fisher, USA) with an accelerating voltage of 200 kV. The TEM images of the brain slices were performed by using a FEI Tecnai G20 TEM (FEI, USA) with an accelerating voltage of 200 kV. Blinded observation of samples with random selection of grid areas was implemented to reduce bias during imaging.

Zeta potential measurement

The zeta potentials of individual AuNCs (50 mg·L^{-1}), Aβ fibrils (pre-incubated from 20 μmol·L^{-1} Aβ_{40}) and Aβ fibrils (20 μmol·L^{-1} Aβ_{40}) together with individual AuNCs (50 mg·L^{-1}) were measured by using a Malvern Nano-ZS ZEN3600 zetasizer.

In vitro inhibition or dissolution experiments

Preparation of Aβ_{40} peptides

All Aβ_{40} peptides used in our experiments were pretreated by 1,1,1,3,3,3-hexafluoro-2-propanol (1 mg·mL^{-1}, $m_{A\beta}/v_{HFIP}$) under the ultrasonic vibration in an ice bath for 2 h. Then, each solution was divided into multiple samples and dried by soft nitrogen airflow respectively. The samples after pretreatment were saved in a refrigerator at -80°C.

Preparation of preformed Aβ_{40} fibril solution

For ThT kinetics and fluorescence imaging, the buffered ThT solution, Aβ_{40} solution (50 μmol·L^{-1}, 100 μL), and ultrapure water were mixed in wells in a certain ratio so that each well contained 60 μmol·L^{-1} ThT, 10 mmol·L^{-1} PBS and 20 μmol·L^{-1} Aβ_{40}. The above solution was pre-incubated for 72 h to form mature fibrils, then different samples (AuNCs or H_2O) were added to each well for further experiments. For CD detection, 200 μL freshly prepared 40 μmol·L^{-1} Aβ_{40} were pre-incubated in a quartz cuvette at 37°C for 48 h to grow mature fibrils. The quartz cuvette was kept in a CD spectrometer, covered with a cap and sealed by sealing film. After the incubation, a 200 μL solution of 100 mg·L^{-1} AuNCs was injected in the quartz cuvette; the concentration of preformed Aβ_{40} fibrils would be diluted twice. Then, the quartz cuvette was sealed again and incubated for further experiments. For cell experiments, a 96-well plate was used to incubate Aβ_{40} fibrils solution. Each well containing buffered Aβ_{40} solution was incubated at 37°C for 48 h to grow mature fibrils. Then, Aβ_{40} fibrils solution, DMEM and AuNCs were mixed in a certain ratio and added into another 96-well plate containing cells. The concentration of preformed Aβ_{40} fibrils would be diluted twice.

The kinetics monitored by ThT assay

The mixtures for ThT assays were incubated at 37°C. All fluorescence data were recorded by using a Synergy^{TM} MX Multi-Mode Microplate Reader with a bottom-reading mode in 96-well flat bottom (Costar) plates sealed with a platemax film. Plates were shaken at medium intensity for 10 s before reading fluorescence data with an excitation wavelength of 445 nm and emission wavelength of 485 nm.

The inhibition effect of different AuNCs on Aβ_{40} fibrillation monitored by ThT assays

A series of working solutions (250 μL) were prepared containing 20 μmol·L^{-1} Aβ_{40} peptides, 20 μmol·L^{-1} ThT in 10 mmol·L^{-1} phosphate buffer (PBS) at pH 7.4 without or with 25 mg·L^{-1} of seven kinds of AuNCs. Fluorescence data were recorded every 10 min. Each experiment was run in sextuplicate in a 96-well plate.

The effect of $Au_{23}(CR)_{14}$ on the disassembly of Aβ_{40} fibrils monitored by ThT

A series of sample solutions (250 μL) were prepared containing 20 μmol·L^{-1} Aβ_{40} peptides, 20 μmol·L^{-1} ThT in 10 mmol·L^{-1} PBS, pH 7.4, at 37°C. The samples were incubated until the fluorescence intensity reached platform (Aβ_{40} fibrils were formed). Then, 10 μL solutions of different mixtures were injected in parallel groups. The samples containing Aβ_{40} fibrils were co-incubated without or with 50 mg·L^{-1} $Au_{23}(CR)_{14}$ for the next 72 h. Fluorescence data were recorded every 10 min.

AFM measurement track morphology change during the dissolution of Aβ_{40} fibrils

AFM experiments were carried out on a FastScan Scanning Probe Microscope (Bruker) with ScanAsyst in air mode and mechanical properties

mode at room temperature. A sample was prepared by dripping 5.0 μL of a solution of the mixture onto freshly cleaved mica and allowing it to dry in the air. Images were conducted with a force constant of 0.225 $N{\cdot}m^{-1}$ and processed by NanoScope analysis software. For AFM track morphology change during the dissolution of Aβ_{40} fibrils, mixtures of 20 $\mu mol{\cdot}L^{-1}$ Aβ_{40} were pre-incubated in 96-well plates at 37°C (in an incubator chamber) for 72 h. Then, 20 μL mixtures of $Au_{23}(CR)_{14}$ were injected into the pre-incubated mixtures of Aβ_{40}. After the incubation of Aβ_{40} fibrils in the presence of 50 $mg{\cdot}L^{-1}$ $Au_{23}(CR)_{14}$ for 0, 3, 6, 12, 24 or 48 h, samples for AFM studies were prepared by dripping 5.0 μL of a solution of the mixture onto freshly cleaved mica.

In situ real-time circular dichroism spectroscopy

CD spectra were recorded in the far-UV region from 190 to 250 nm by a JASC J-1500 Spectrometer, using a setup containing a step of 0.5 nm, a bandwidth of 1.0 nm, a speed of 50 $nm{\cdot}min^{-1}$, a time per point of 1.0 s, an ultrasonic vibration of 600 rpm and an incubation temperature of 37°C. The sample for experiment was collected in a quartz cuvette with a 1 mm optical path length; the cuvette was covered with a cap and sealed by sealing film. Each spectrum calibrated after subtraction of background signal was processed with a smoothing function of 30 points. The spectra data were recorded every 3 h.

DLS tracks apparent size change during the dissolution of Aβ_{40} fibrils

DLS measurement was performed on a Malvern Nano-ZS ZEN3600 zetasizer. Mixtures of 20 $\mu mol{\cdot}L^{-1}$ Aβ_{40} were pre-incubated in a high-quality quartz glass cuvette at 37°C (in an incubator chamber) for 72 h. Then, 20 μL mixtures of $Au_{23}(CR)_{14}$ were injected into the pre-incubated mixtures of Aβ_{40} and incubated for another 48 h. The apparent size of the sample was recorded at the 0, 3rd, 6th, 12th, 24th and 48th hour.

Native PAGE

The Aβ states after co-incubation with or without $Au_{23}(CR)_{14}$ were analysed via Native PAGE using 4–20% Tris-glycine gradient gels (BeyoGel). Native PAGE (no addition of β-mercaptoethanol and SDS) was adopted here for maintaining non-covalent bonds of samples. Samples of Aβ fibrils with or without $Au_{23}(CR)_{14}$ (50 $mg{\cdot}L^{-1}$) were added to native loading buffer. Equal volumes of each sample (20 μL) were loaded onto gels along with BeyoColor (Beyo) prestained molecular weight markers and electrophoretically separated at 150 V. Gels were stained for total protein using a hypersensitivity Coomassie blue (BeyoBlue) according to the manufacturer's protocol. After incubation with decoloring solution three times (each for 3 h), the gel was detected by the gel imaging analysis system.

Cell experiments

PC-12 cells were incubated in DMEM medium supplemented with 10% fetal bovine serum (FBS) at 37°C with 5% CO_2. The cells were regularly subcultured to maintain them in logarithmic phase of growth. The cells were seeded in 96-well plates at a cell population of ~10 000 cells per well and incubated for 24 h at 37°C before further treatment. The viability of PC-12 cells was assessed by CCK-8 assay. Before being examined by using a Synergy™ MX Multi-Mode Microplate Reader at a wavelength of 450 nm, cells were treated with 100 mL DMEM contained 10% CCK-8 solution for ~2 h.

Cytotoxicity test of $Au_{23}(CR)_{14}$

Cells of the blank controls were incubated with fresh DMEM, the cells of the experiment group were incubated with DMEM containing different doses of $Au_{23}(CR)_{14}$ (1, 10, 25 and 50 $mg{\cdot}L^{-1}$) for 24 h. The viability of PC-12 cells was assessed by CCK-8 assay.

Preformed Aβ_{40} fibril-lesioned PC-12 cell model

To investigate the effect of the 50 $mg{\cdot}L^{-1}$ $Au_{23}(CR)_{14}$-mediated dissolution process of Aβ_{40} fibrils on cell viabilities, the PC-12 cells of the experiment group were incubated with DMEM containing preformed Aβ_{40} fibrils and 50 $mg{\cdot}L^{-1}$ $Au_{23}(CR)_{14}$ for 3, 6, 12, 24 or 48 h, respectively. Five 96-well plates containing PC-12 cells, preformed Aβ_{40} fibrils and 50 $mg{\cdot}L^{-1}$ $Au_{23}(CR)_{14}$ were prepared for the five time points cell experiments. The PC-12 cells of the five experiment groups were incubated for 3, 6, 12, 24 or 48 h, respectively. Each 96-well plate was examined once. Cells of the blank controls were incubated with fresh DMEM. The viabilities of PC-12 cells were assessed by CCK-8 assay.

In situ cell imaging monitoring

In situ bright field cell images were recorded by using a Cytation™ 5 Cell Imaging Multi-Mode Reader (BioTek). The PC-12 cells were co-incubated with preformed Aβ_{40} fibrils in the absence or presence of 50 $mg{\cdot}L^{-1}$ $Au_{23}(CR)_{14}$ in 96-well plates at 37°C with 5% CO_2 for 48 h. The *in situ* real-time cell images were recorded every 1 h.

Immunohistochemical analyses of brain slices

The APP/PS1 Tg mice were anesthetized with 7% chloral hydrate, and transcardially perfused with phosphate-buffered saline (PBS, pH 7.4) followed by 4% paraformaldehyde in PBS. After perfusion fixation, the mouse brains were removed and fixed overnight in 4% paraformaldehyde at 4°C. Then the brains were dehydrated with 30% sucrose in PBS solution. Coronal slices (8 μm) containing both the neocortex and hippocampus were cut on a CM 1950 (Leica) freezing microtome. The brain slices were co-incubated without (blank control) or with $Au_{23}(CR)_{14}$ for 48 h. Then the slices were incubated with the primary mouse anti-Aβ antibody (Abcam, 1:100) followed by a horseradish peroxidase Goat Anti-Rabbit secondary antibody (Abcam). After washing, the slices were stained by using diaminobenzidine and counter-stained by hematoxylin, and observed by using an BX53 biological microscope (Olympus).

$Au_{23}(CR)_{14}$ across the blood–brain barrier

To investage whether the $Au_{23}(CR)_{14}$ could cross the blood–brain barrier, 20 mg·kg^{-1} $Au_{23}(CR)_{14}$ (dissolved in normal saline) was slowly injected into the caudal vein of the laboratory mice for a period of less than 20 s. The mice were sacrificed by cervical dislocation 6 h later. The brains were quickly collected on ice and then fixed immediately by 2.5% glutaraldehyde fixative. Subsequently, 10% osmium tetroxide was used to further fix the brains. Then the brains were embedded in paraffin and sectioned into 80–100 nm slices by using an EM UC7 (Leica) ultramicrotome. Finally, the brain slices were used for analysis of the presence of $Au_{23}(CR)_{14}$ by TEM.

SUPPLEMENTARY DATA

Supplementary data are available at *NSR* online.

FUNDING

This work was supported by the National Natural Science Foundation of China (21975191, 21805218, 51873168, 81803515, 51533007 and 51521001), the Natural Science Foundation of Hubei Province (2018CFA002 and 2018CFB348), Wuhan University of Technology fund for first-class university, first-class discipline construction projects (472-20162008), Fundamental Research Funds for the Central Universities (WUT: 2018III023) and Excellent Dissertation Cultivation Funds of Wuhan University of Technology (2017-YS-010).

Conflict of interest statement. None declared.

REFERENCES

1. Rocker A, Roan NR and Yadav JK *et al.* Structure, function and antagonism of semen amyloids. *Chem Commun* 2018; **54**: 7557–69.
2. Sorrentino V, Romani M and Mouchiroud L *et al.* Enhancing mitochondrial proteostasis reduces amyloid-β proteotoxicity. *Nature* 2017; **552**: 187–93.
3. Jucker M and Walker LC. Amyloid-β pathology induced in humans. *Nature* 2015; **525**: 193–4.
4. Xin Y, Wang X and Luo L *et al.* Conformation-dependent manipulation of human islet amyloid polypeptide fibrillation by shiitake-derived lentinan. *ACS Appl Mater Interfaces* 2018; **10**: 31069–79.
5. Ruggeri FS, Adamcik J and Jeong JS *et al.* Influence of the β-sheet content on the mechanical properties of aggregates during amyloid fibrillization. *Angew Chem Int Ed* 2015; **54**: 2462–6.
6. Furtado D, Bjornmalm M and Ayton S *et al.* Overcoming the blood-brain barrier: the role of nanomaterials in treating neurological diseases. *Adv Mater* 2018; **30**: 1801362.
7. Ban DK and Paul S. Nano zinc oxide inhibits fibrillar growth and suppresses cellular toxicity of lysozyme amyloid. *ACS Appl Mater Interfaces* 2016; **8**: 31587–601.
8. Brahmachari S, Arnon ZA and Frydman-Marom *et al.* Diphenylalanine as a reductionist model for the mechanistic characterization of β-amyloid modulators. *ACS Nano* 2017; **11**: 5960–9.
9. Mishra R, Bulic B and Sellin D *et al.* Small-molecule inhibitors of islet amyloid polypeptide fibril formation. *Angew Chem Int Ed* 2008; **47**: 4679–82.
10. Gupta J, Fatima MT and Islam Z *et al.* Nanoparticle formulations in the diagnosis and therapy of Alzheimer's disease. *Int J Biol Macromol* 2019; **130**: 515–26.
11. Ye L, Fritschi SK and Schelle J *et al.* Amyloid-β pathology induced in humans. *Nat Neurosci* 2015; **18**: 1559–61.
12. Liu Y, Giunta B and Zhou H *et al.* Immunotherapy for Alzheimer disease the challenge of adverse effects. *Nat Rev Neurol* 2012; **8**: 465–9.
13. Kumar S, Henning-Knechtel A and Chehade I *et al.* Foldamer-mediated structural rearrangement attenuates Aβ oligomerization and cytotoxicity. *J Am Chem Soc* 2017; **139**: 17098–108.
14. Niu L, Liu L and Xi W *et al.* Synergistic inhibitory effect of peptide-organic coassemblies on amyloid aggregation. *ACS Nano* 2016; **10**: 4143–53.
15. Gao G, Zhang M and Lu P *et al.* Chirality-assisted ring-like aggregation of Aβ(1-40) at liquid-solid interfaces: a stereoselective two-step assembly process. *Angew Chem Int Ed* 2015; **54**: 2245–50.
16. Ke PC, Pilkington EH and Sun Y *et al.* Mitigation of amyloidosis with nanomaterials. *Adv Mater* 2019; doi: 10.1002/adma.201901690.
17. Faridi A, Sun Y and Okazaki Y *et al.* Mitigating human IAPP amyloidogenesis *in vivo* with chiral silica nanoribbons. *Small* 2018; **14**: 1802825.
18. Pilkington EH, Lai M and Ge X *et al.* Star polymers reduce islet amyloid polypeptide toxicity via accelerated amyloid aggregation. *Biomacromolecules* 2017; **18**: 4249–60.

19. Wang M, Sun Y and Cao X. Graphene quantum dots against human IAPP aggregation and toxicity *in vivo*. *Nanoscale* 2018; **10**: 19995–20006.
20. Zhu L, Song Y and Cheng PN *et al.* Molecular design for dual modulation effect of amyloid protein aggregation. *J Am Chem Soc* 2015; **137**: 8062–8.
21. Palmal S, Maity AR and Singh BK *et al.* Inhibition of amyloid fibril growth and dissolution of amyloid fibrils by curcumin-gold nanoparticles. *Chem Eur J* 2014; **20**: 6184–91.
22. Song Y, Moore EG and Guo Y *et al.* Polymer-peptide conjugates disassemble amyloid β fibrils in a molecular-weight dependent manner. *J Am Chem Soc* 2017; **139**: 4298–301.
23. Javed I, Sun Y and Adamicik J *et al.* Cofibrillization of pathogenic and functional amyloid proteins with gold nanoparticles against amyloidogenesis. *Biomacromolecules* 2017; **18**: 4316–22.
24. Ehrnhoefer D, Bieschke J and Boeddrich A *et al.* EGCG redirects amyloidogenic polypeptides into unstructured, off-pathway oligomers. *Nat Struct Mol Biol* 2008; **15**: 558–66.
25. Palhano FL, Lee J and Grimster NP *et al.* Toward the molecular mechanism(s) by which EGCG treatment remodels mature amyloid fibrils. *J Am Chem Soc* 2013; **135**: 7503–10.
26. Kakinen A, Adamcik J and Wang B *et al.* Nanoscale inhibition of polymorphic and ambidextrous IAPP amyloid aggregation with small molecules. *Nano Res* 2018; **11**: 3636–47.
27. Li J, Chen R and Zhang S *et al.* Chiral effect at nano-bio interface: a model of chiral gold nanoparticle on amylin fibrillation. *Nanomaterials* 2019; **9**: 412.
28. Gao G, Chen R and He M *et al.* Gold nanoclusters for Parkinson's disease treatment. *Biomaterials* 2019; **194**: 36–46.
29. Zhang M, Mao X and Yu Y *et al.* Nanomaterials for reducing amyloid cytotoxicity. *Adv Mater* 2013; **25**: 3780–801.
30. Chevrier DM, Raich L and Rovira C *et al.* Molecular-scale ligand effects in small gold-thiolate nanoclusters. *J Am Chem Soc* 2018; **140**: 15430–6.
31. Gao G, Zhang M and Gong D *et al.* Size-effect of gold nanoparticles and nanoclusters to inhibit amyloid-β fibrillation. *Nanoscale* 2017; **9**: 4107–13.
32. Xiong N, Zhao Y and Dong X *et al.* Design of a molecular hybrid of dual peptide inhibitors coupled on AuNPs for enhanced inhibition of amyloid β-protein aggregation and cytotoxicity. *Small* 2017; **13**: 1601666.
33. Wallin C, Hiruma Y and Warmlander S *et al.* The neuronal tau protein blocks *in vitro* fibrillation of the amyloid-β (Aβ) peptide at the oligomeric stage. *J Am Chem Soc* 2018; **140**: 8138–46.
34. Gobbi A and Frenking GY. Conjugated compounds: the equilibrium geometries and electronic structures of guanidine, guanidinium cation, urea, and 1,1-diaminoethylene. *J Am Chem Soc* 1993; **115**: 2362–72.
35. Chowdhury SR, Agarwal M and Meher N *et al.* Modulation of amyloid aggregates into nontoxic co-aggregates by hydroxyquinoline appended polyfluorene. *ACS Appl Mater Interfaces* 2016; **8**: 13309–19.
36. Laganowsky A, Liu C and Sawaya MR *et al.* Atomic view of a toxic amyloid small oligomer. *Science* 2012; **335**: 1228–31.
37. Benilova I, Karran E and De-Strooper B. The toxic Aβ oligomer and Alzheimer's disease: an emperor in need of clothes. *Nat Neurosci* 2012; **15**: 349–57.
38. Hu J, Gao G and He M *et al.* The optimal route of gold nanoclusters administration in mice targeting Parkinson's disease. *Nanomedicine* 2019; doi: 10.2217/nnm-2019-0268.
39. Javed I, Peng G and Xing Y *et al.* Inhibition of amyloid beta toxicity in zebrafish with a chaperone-gold nanoparticle dual strategy. *Nat Commun* 2019; **10**: 3780.
40. Qing G, Lu Q and Li X *et al.* Hydrogen bond based smart polymer for highly selective and tunable capture of multiply phosphorylated peptides. *Nat Commun* 2017; **8**: 461.